Nanoscale
Advances

ROYAL SOCIETY
OF CHEMISTRY

PAPER

View Article Online
View Journal | View Issue

Check for updates

Cite this: *Nanoscale Adv.*, 2020, **2**, 4841

Core–shell Au@AuAg nano-peanuts for the catalytic reduction of 4-nitrophenol: critical role of hollow interior and broken shell structure†

Varsha Thambi,[a] Abhay Raj Singh Gautam[b] and Saumyakanti Khatua *[a]

Received 20th April 2020
Accepted 17th August 2020

DOI: 10.1039/d0na00312c

rsc.li/nanoscale-advances

Bimetallic hollow core–shell nanoparticles have gained immense attention, especially as a high-performance catalyst due to their large surface area and increased number of uncoordinated atoms. However, the synthesis of an anisotropic hollow structure with large number of uncoordinated atoms and tailored hole size remains elusive. Herein, we report the synthesis of peanut-like core–shell nanostructures consisting of Au nanorods as the core covered by the AuAg alloy shell. The AuAg shell was formed on the Au nanorod core *via* co-deposition of Ag and Au atoms without disturbing the Au nanorod core. Then, we controllably and selectively removed Ag atoms from the shell to create "Broken Shell Peanuts" with variable hole size between 8 ± 4 nm and 26 ± 7 nm. Further, we utilized these nanostructures with different hole size as catalysts to reduce 4-nitrophenol to 4-aminophenol where the broken shell peanut nanostructures with a hole size of 26 ± 7 nm were found to be 12 times more efficient than the solid shell peanut structures.

1 Introduction

Plasmonic nanoparticles are extensively studied due to their intriguing size and shape-dependent optical and electrical properties.[1] These properties of metal nanoparticles arise from their collective resonant oscillation of conduction electrons giving rise to the surface plasmon resonance (SPR).[2,3] The SPR allows them to interact and manipulate light at the nanoscale level, making them useful in a number of applications including surface-enhanced Raman scattering (SERS),[4] plasmon-enhanced solar cells,[5] photodetectors,[2] and therapeutics.[6] In recent years, metal nanoparticles have also been extensively utilized as catalysts in plethora of reactions comprising homogeneous catalysis,[7] photo-catalysis,[8] total synthesis,[9] anaerobic,[10] and oxidation reactions.[11]

Further, metal nanoparticles (MNP) with a hollow structure have been known for even better catalytic properties.[12,13] The enhanced catalytic activity of these hollow MNPs compared to their solid counterparts with larger density is due to the enormous increase in their surface to volume ratio.[14] Apart from the morphology, the composition of nanoparticles also influences their catalytic property. Various AgAu bimetallic hollow nanostructures such as nanosphere,[15,16] nanocubes,[17–19] nanowires,[20] nanorods,[14] nanotubes,[21] nanoshells,[22] nanobowls,[23] and nanoframes[24] are highly efficient in various catalytic reactions such as the reduction of nitrophenol,[14] degradation of methylene blue,[25] aniline oxidation,[24] and oxidation of various organic molecules.[26] Zheng *et al.* compared Au nano boxes with their hollow counterpart "nanocages" and reported them as catalytically more active.[27] Such an activity was directly related to their morphology with ultra-thin walls and holes on the surface that provide accessibility to active sites present both inside and outside the nanocage structure. Wu *et al.* found a similar effect in the hollow nanostructure, suggesting the influence of hollowness and morphology on their enhanced activity.[28] El-Sayed and their co-workers attributed the enhanced activity of their hollow NS to an effect called the "Cage effect", where the catalytic reaction proceeds inside the cage.[29,30] They suggested that certain conditions are required to obtain the best possible reaction rates in the nanocage, which are: (i) the hole size should be large enough to allow the reactant molecules to diffuse in and out of the cage, and at the same time, should be small enough to keep the steady-state concentration of radicals; (ii) the hole size inside the structure should be large enough to provide optimum collision rate of the reactant molecules. Thus, apart from the morphology and composition of hollow nanoparticles, the hole size plays a key role in achieving the highest catalytic activity.[31]

Hollow bimetallic NPs are mainly prepared using template-like silica beads, polymer latexes, or solid metal NPs. Typically, a thin shell of the desired metal is deposited on top of the sacrificial template, and subsequently, the template is removed using a selective removal process of dissolution using wet

---

[a] *Discipline of Chemistry, Indian Institute of Technology Gandhinagar, Gujarat, India. E-mail: khatuask@iitgn.ac.in*

[b] *Discipline of Material Science and Engineering, Indian Institute of Technology Gandhinagar, Gujarat, India*

† Electronic supplementary information (ESI) available. See DOI: 10.1039/d0na00312c

chemical etching or calcination.[32] Many self-template methods also exist that use processes such as galvanic replacement,[23] Kirkendall effect,[33,34] de-alloying,[35,36] and Ostwald ripening to synthesize the hollow nanostructures.[37] The galvanic replacement technique involves the substitution of more noble ions present in the solution with the less noble metal present on the surface of the structure, whereas the dealloying technique utilizes acidic conditions for the removal of less noble metal from the nanostructure. On the other hand, the Kirkendall effect originates from the difference in the diffusion rates between two components, which leads to the creation of vacancies on the nanostructure, thereby creating a hollow nanostructure.[38] On the other hand, in Ostwald ripening, smaller crystals from the surface diffuse out and allow larger crystals from the solution to deposit on the structure.[37] This phenomenon works on the principle that large particles are thermodynamically more favorable for deposition and small particles have a higher solubility than the large ones. In these techniques, the void shape and size of the hollow NS prepared are determined by the nature of the template, while the resultant composition and the morphology of the shell are determined by the coating and removal process.[31] With the above techniques, many core–shell bimetallic hollow nanostructures have also been synthesized. These hollow core–shell NS are even more catalytically active compared to the hollow NS as it provides an extra metallic core layer along with a hollow outer shell, which allows the reactant molecules to be catalyzed by the metals present in the inside core, as well as on the inner and outer walls of the nanoparticles.[26] Therefore, these structures not only provide high surface area, but the porosity present in these structures can trap the reactant molecules within their cavity for a longer duration, which in turn increases the rate of the catalytic reaction.[39] In spite of the simplicity and versatility in their templating strategy, wet chemical synthesis of these core–shell hollow bimetallic nanostructures is limited to spherical and rod shape only[40–42] and the synthesis of complex and high faceted nanostructures with precise control over the hole size remains a challenge.

In this work, the peanut-shaped core–shell NS were synthesized by the simultaneous deposition of Ag and Au atoms on Au nanorods. Such Au@AuAg structures are different from previously reported NPs with Au core–AuAg shell structure.[43–49] Further, on treatment with HCl, this peanut structure transforms into a hollow core–shell broken shell peanut structure. With time, the peanut structure develops small pinholes on the walls of the structure, which then evolve into bigger holes, which allow the atoms from the inside to diffuse out of the structure, thus creating a hollow interior. This transformation of the peanut to broken shell peanut structure during the reaction is due to the dealloying effect. Also, we were able to tune the hole size of the broken shell nano-peanut structures between 8 ± 4 and 26 ± 7 nm simply by quenching the reaction at different time intervals of 30 min and 60 min, respectively. Furthermore, we used these hollow nanostructures to catalyze the reduction of 4-nitrophenol to 4-aminophenol. The rate of reaction catalysed by the broken shell nano-peanut structure with a hole size of 26 ± 7 nm was found to be 12 times higher than the peanut structure with no holes. The higher catalytic activity is attributed to the ability of 4-nitrophenol to interact with the Au atoms not only present in the outer shell but also allow it to enter inside the structure and interact with the atoms present both inside the shell and on the nanorod lying inside the shell.

2 Experimental section

2.1 Chemicals and instrumentation

Silver nitrate ($AgNO_3$), gold(III) chloride trihydrate ($HAuCl_4 \cdot 3H_2O$), and sodium borohydride ($NaBH_4$) were bought from Sigma Aldrich. Hydroquinone (HQ, 99%) was purchased from Alfa Aesar. Sodium hydroxide pellets and hydrochloric acid (35–37%) were purchased from Rankem. All chemicals were used as received without any further purification. Ultra-pure water (18.2 MΩ cm^{-1}) was used in all the synthesis.

All extinction spectra were recorded using a V-750 JASCO UV-visible spectrophotometer in a 1 cm quartz cuvette at room temperature (25–28 °C). Scanning electron microscopy (SEM), in combination with energy-dispersive X-ray spectroscopy (EDS), was done using SEM (SM-7600F Schottky Field Emission Scanning Electron Microscope from JEOL) at 15 kV. For all length-related histograms, a minimum of 100 particles were measured to obtain the average size distribution using ImageJ software. Transmission electron micrographs (TEM) were acquired using a Tecnai F30 field emission microscope, where the sample was drop-casted on a 300-mesh copper grid. Inductively Coupled Plasma-Optical Emission Spectroscopy (ICP-OES) data were recorded using an Avio 200-ICP-OES by PerkinElmer. X-ray Photoelectron Spectroscopy (XPS) was carried out using a PHI 5000 Versa prob II, FEI Inc.

2.2 Synthesis of gold nanorods

(a) Preparation of seeds: the seed solution was prepared by adding $HAuCl_4 \cdot 3H_2O$ (5 mL, 1 mM) to CTAB (5 mL, 0.2 M) solution, which was then stirred for two minutes. Then, the reducing agent, $NaBH_4$ (800 μL, 0.01 M), was quickly added to the solution under vigorous stirring. The color of the seed solution turned brown instantly. The seed solution was then kept undisturbed for 30 minutes. (b) Preparation of the growth solution: the growth solution was prepared by adding $AgNO_3$ (625 μL, 40 mM) to CTAB (50 mL, 0.1 M) solution. The solution was stirred for a minute and then kept undisturbed for 15 minutes. Then, $HAuCl_4 \cdot 3H_2O$ (500 μL, 100 mM) was added to the solution and the solution was stirred for another 5 minutes. Then, 600 μL of 0.5 M hydroquinone was added to the solution, followed by 1 mL of the seed solution. The mixture was stirred for a few minutes and then kept undisturbed overnight at 28 °C. The mixture was kept for 12 hours before centrifugation and then the precipitate was re-dispersed in 200 μM CTAB.

2.3 Preparation of the peanut nanostructure

The growth solution was prepared by adding $AgNO_3$ (1 mL, 40 mM) in CTAB (100 mL, 0.1 M), and the solution was kept undisturbed for 15 minutes. Then, $HAuCl_4 \cdot 3H_2O$ (100 mM, 100 μL) was added to the above solution and sonicated until the solution became clear. After that, to increase the pH of the solution (pH = 8), NaOH (1 mL, 0.1 M) solution was added to the growth solution. Then, hydroquinone (0.5 M, 2 mL) was added to the growth solution, which changed the color of the solution to colorless, followed by the addition of 750 μL of the nanorod solution (to make the optical density of the nanorod in the whole solution ~0.24). The mixture was kept for 10 hours at 28 °C before centrifugation and then the precipitate was redispersed in 200 μM CTAB.

2.4 Synthesis of broken shell peanut

HCl (12 M, 300 μL) was added to 10 mL of 0.1 M CTAB solution. Then, 500 μL of the nanostructure was added to the above mixture (to make the optical density of the peanut structure in the solution ~0.7). The mixture was kept undisturbed for 6 hours at 28 °C before centrifugation, and then the precipitate was redispersed in 200 μM CTAB.

2.5 Reduction of 4-nitrophenol

1 mL of 0.1 M $NaBH_4$ was added to 2 mL of 0.01 M 4-NP. The solution was stirred for a minute and then a definite amount of the nanostructure was added to the above solution. The reduction was monitored *via* a UV-Visible spectrometer.

4 Result and discussion

The broken shell peanut structure was obtained in three steps, as shown in Scheme 1. Firstly, gold nanorods were synthesized by the seed-mediated method using hydroquinone as a reducing agent (refer to the Experimental section). The nanorods were formed with an average length and width of 70.7 ± 17 nm and 15 ± 2 nm, respectively (Fig. S1(a–c)†). Secondly, these nanorods were grown into the peanut-like structure by overgrowing the nanorods at pH = 8. The nanorods grew into the nano-peanut structure with an average length and width of 97.2 ± 9 nm and 42.7 ± 3 nm, respectively (Fig. S1(d–f)†). Finally, these nano-peanuts were mixed in a solution containing 0.33 M HCl in the presence of CTAB to obtain a broken shell peanut-like structure with an average length and width of 81.3 ± 12 nm and 40.8 ± 3 nm, respectively (Fig. S1(g–i)†).

The extinction spectra and the corresponding images of the nanorod, peanut, and the broken shell peanut are shown in Fig. 1a–d. The extinction spectra of the nanorods show Longitudinal Surface Plasmon Resonance (LSPR) at 840 nm and Transverse Surface Plasmon Resonance (TSPR) at 520 nm (blue spectra, Fig. 1a). The overgrowth of nanorods causes a large blue shift of 195 nm in the LSPR position (magenta, Fig. 1a), indicating an overall decrease in the aspect ratio. This was confirmed by the SEM images, where the aspect ratio decreases from 4.7 to 2.3. The TEM image of the overgrown structure suggests the isotropic deposition of metal on the Au nanorod structure, further suggesting the decrease in the aspect ratio (Fig. 1c, inset). It is to be noted that not just LSPR but the TSPR position of the nano-peanut structure is also blue shifted by 45.5 nm and falls at about 466 nm. It is known that the TSPR of a pure gold nanorod is observed in the range from 504 to 530 nm. On the other hand, the Ag nanoparticles exhibit TSPR at $\lambda < 500$ nm.[22] This suggests that the nano-peanut consists of both Ag and Au atoms. Here, the overgrowth of the nanorod to the peanut structure was performed at pH = 8 (refer to the Experimental section). The high pH of the growth solution allows the simultaneous deposition of Au and Ag on the Au nanorods.[50] The incorporation of Ag during the growth of the peanut structure was probed by three techniques: X-ray photoelectron spectroscopy (XPS) (Fig. S2(a and b)), Inductively Coupled Plasma-Optical Emission Spectrometry (ICP-OES) (green, Fig. S2(c)), and Energy Dispersive X-ray Spectroscopy (EDS) (blue, Fig. S2(c)) (Table S1).† All three techniques confirmed the presence of both Ag and Au in the peanut structure. The ICP-OES analysis showed the presence of 76.6 atomic% of Ag and 23.4 atomic% of Au in the peanut structure, contrary to the nanorods, which were constituted of mostly Au (atomic percentage of 97%). Further, the transmission electron microscope (TEM) image of the peanut structure showed a well-defined core–shell bimetallic structure (inset of Fig. 1c). The high contrast in the TEM image at the centre compared to the outer structure of the peanut (Fig. 1c, inset) indicates that the Ag–Au alloy formation has taken place only in the shell structure, while the shape of the core of peanut, *i.e.*, the nanorods, remains unaffected during overgrowth. Xie *et al.* reported the formation of nano-peanut-like structures by first depositing Ag shell on the Au core to form the nanosphere structure, and then the same Ag shell was galvanically replaced in the presence of gold chloride and citrate solution to form peanut-like structures.[51] The growth conditions allowed the Au atoms to fully replace the Ag atoms and to develop a new protuberance on

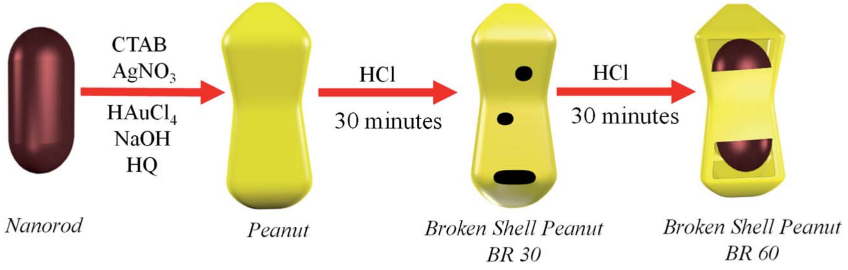

Scheme 1 Schematic description of steps involved in the formation of the peanut nanostructure by overgrowth and their transformation into hollow core–shell broken shell peanut nanostructures by the dealloying effect at 30 minutes (BR 30) and 60 minutes (BR 60).

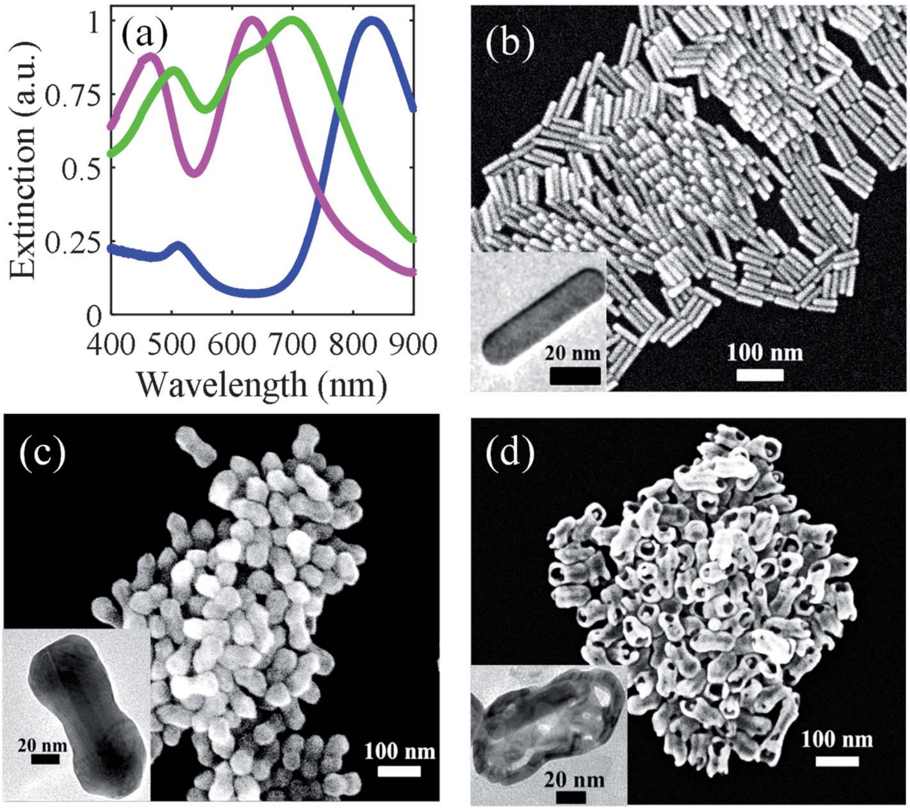

Fig. 1 (a) Extinction spectra of the nanorod (blue), peanut (magenta), and broken shell peanut (green), and the corresponding SEM images and TEM image (in the inset) of the nanorod (b), peanut (c), and broken shell peanut (d).

each of the Au core spheres to form the peanut structure with no Ag content. Kou *et al.* in their work overgrew Au nanorods to form the Au nano-peanuts in the presence of glutathione or cysteine.[52] The binding of glutathione/cysteine at the ends of the nanorods allowed the deposition of Au, first at the corners, giving a peanut kind of shape, and further deposition takes place at the lateral side, thus changing the peanut shape to an octahedral shape. The peanut structure formed in their work was made entirely of Au atoms. Similarly, Song *et al.* grew Au@Au nanorods in the presence of CTAB to obtain a dumbbell-shaped Au peanut structure made only of Au atoms with no core–shell morphology.[53] Contrary to the reported work, we have deposited both Au and Ag on the gold nanorods at pH 8 in the presence of CTAB to obtain the nano-peanut structure. Our group has previously reported the importance of maintaining the pH of the growth solution, as a differently shaped nanostructure can be obtained by varying the pH of the growth solution and keeping all the other growth parameters constant.[50] The growth at pH 8 allowed the formation of the shell structure consisting of both Ag and Au, while the core structure remained purely Au. The presence of both Ag and Au in the shell were essential in this work to obtain the broken shell peanut structure, which is discussed below in detail.

The transformation of the nano-peanut to a broken shell peanut structure causes mainly two changes in the spectra (green, Fig. 1a). Firstly, both the LSPR and TSPR positions shift to higher wavelength, and secondly, it also causes the concomitant broadening of the LSPR peak. This broadening of the LSPR is consistent with the formation of holes in the structure, which is also visible in the SEM image in Fig. 1d. It is possible that instead of two modes that were observed in the nanorod and peanut structure, the plasmon broadens due to the overlapping of several modes arising from multiple resonances from the holes that are present on the structure.[54] Further, this broken shell peanut structure shows a decrease in the molar ratio of Ag, which is confirmed both by ICP-OES and EDS measurements (Table S1 and Fig. S2(c)†), where the atomic percentage of Ag reduces to 46% (calculated by ICP-OES). The shift of TSPR to a higher wavelength also indicates the removal of Ag from the original peanut structure. This transformation leads to the formation of large holes on the surface of the peanut structure. The SEM image in Fig. 1d shows hollowness inside the structure and the nanorod lying inside the outer shell. Moreover, the TEM image in the inset of Fig. 1d shows that the nanorod has moved to one end of the broken shell peanut structure, which indicates that the nanorod can freely move inside this broken shell peanut structure.

To understand the mechanism involved in the formation of the broken shell peanut structures, we examined the time-dependent evolution of the holes in the peanut structure by monitoring the extinction spectra and the SEM/TEM images by centrifuging the sample at different time intervals. This allowed us to kinetically trap these nanoparticles in their intermediate structures and allowed the study of hole formation and change in their composition over time. During the transformation, both the LSPR and TSPR peaks first decreased in intensity and then gradually shifted towards higher wavelength (Fig. 2a). Initially, at 0 minutes, the peanut structure shows well defined core–shell morphology, as shown in Fig. 2b and c. The average thickness of the peanut shell is 21 ± 2 nm (Fig. 2j). Within 30 minutes of the reaction, multiple small holes start appearing on the surface of the nano-peanut (Fig. 2d and e). These holes then become larger with time, and after 60 minutes, the nanorod core becomes visible through these holes (Fig. 2f and g). The hole size increases from 8 ± 4 nm (yellow histogram in Fig. 2n) at 30 minutes to 26 ± 7 nm (green histogram in Fig. 2n) at 60 minutes. This larger shift in hole size within half an hour is because the smaller holes, which were located all over the surface (refer to Fig. 2d), merge to create a bigger hole that segregates at one location (refer to Fig. 2f). Here, the hole size was measured by plotting the intensity line profile of the selected region in ImageJ software, as shown in Fig. 2l and m. The average hole size was measured at 30 minutes and 60 minutes on 100 particles. With time, the outer shell of the peanut structure becomes thin, and in many cases, the inner nanorod core comes out of the outer shell (Fig. 2h and i).

The crystallographic structures of the nanoparticles, *i.e.*, nanorod, peanut (BP 0), and broken shell peanut structure were determined by a combination of HRTEM and FFT spot pattern (Fig. S3(I–IV)†). As shown in Fig. S3(I),† the nanorod length direction is aligned with the {100} crystallographic direction of the Au nanorod. In addition, the [110] oriented nanorods also

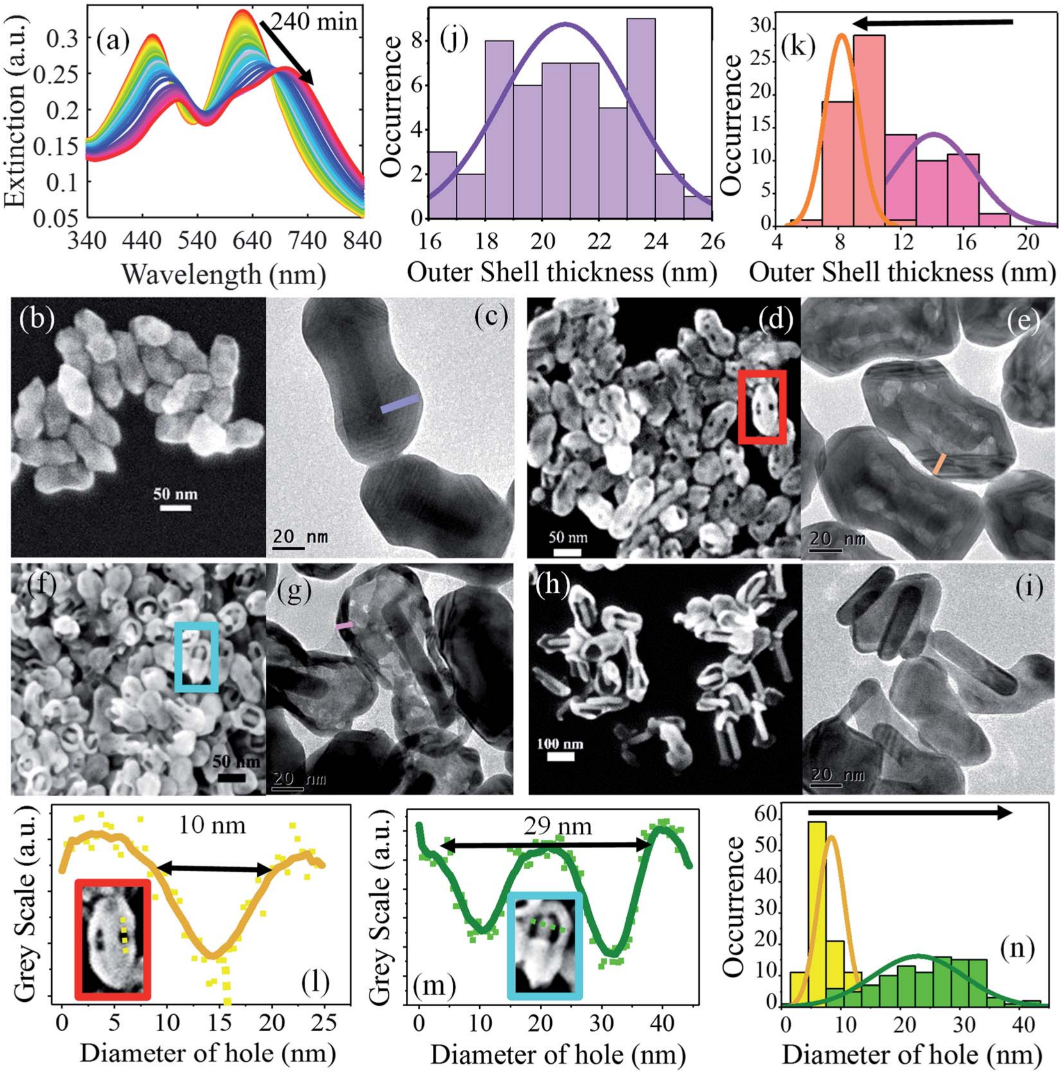

Fig. 2 (a) Time-dependent evolution of the extinction spectra in the presence of 0.33 M HCl where both LSPR and TSPR shift to higher wavelength with time. (b, d, f and h) SEM image of the sample at 0, 30, 60, and 240 minutes, respectively. (c, e, g and i) TEM image of the sample at 0, 30, 60, and 240 minutes, respectively. (j) Histogram distribution of the outer shell (purple line in (c)) of the average length of 21 ± 2 nm. (k) Histogram distribution of the outer shell thickness reduces from 13 ± 2 nm (magenta) at 30 minutes to 8 ± 2 nm (red) at 60 minutes. (l and m) Intensity line profile of the red and cyan selected area of (d) and (f) where the dip in the curve indicates the presence of holes of dimension of 10 nm and 29 nm. (n) Histogram distribution of the diameter of holes with the dimension of 8 ± 4 nm (yellow) at 30 minutes to 26 ± 7 nm (green) at 60 minutes.

provide clear evidence of faceting along the {111} planes at the tip in these nanorods. However, we do not see any clear signs of faceting in the lateral direction based on our observation of various oriented nanorods. Similarly, the peanut structures seem to grow on these nanorod precursors using them as a crystallographic template. As shown in the images in Fig. S3(II)† and corresponding FFT of the [110] oriented peanut structure, the growth direction of {100} is preserved while the {111} faceting is now much more pronounced than that in case of gold nanorods, as indicated by longer facets at the tip. Also, laterally, the particle still did not show any sign of faceting along any preferred crystallographic plane. From the peanut to the broken shell peanut transformation, we observe anisotropic leaching where the tip leaches ∼16 nm, while not much change is observed at the sides (∼2 nm) (Fig. S1g–i†). Here, we do not know the actual role of the crystal planes in the effective leaching of tips and this will be taken up in our future study. But, similar to our work, the group of Chen also found a reduction in the size of the nanostructure due to the removal and rearrangement of atoms after dealloying.[55]

The evolution of holes suggests that some atoms from the peanut structure come out in the solution. There can be two possibilities associated with the diffusion of atoms. Either both Au and Ag are diffusing out of the solution, or only one of the atoms (Au/Ag) is preferentially coming out of the structure. To confirm this, we performed ICP-OES of the nanostructure by centrifuging the sample and digesting it in aqua regia at different time intervals. We found the latter case to be accurate, *i.e.*, only Ag atoms were diffusing out of the system while Au remains the same throughout the whole process (Fig. S4†). In the presence of HCl, Ag ions from the peanut structure diffuse out, creating holes on the walls of the surface through a process called dealloying. This dealloying process always favors the diffusion of the less noble atom (here, Ag) out of the structure, leaving behind the more noble atom (Au).[56] The holes formed on the surface then allow the Ag atoms from inside the layers to come out, creating a hollow interior. This effect becomes prominent when the average outer shell thickness (purple line in Fig. 2c) in the peanut structure of 21 ± 2 nm (Fig. 2j) reduces to 13 ± 2 nm (red) at 30 minutes and 8 ± 2 nm (magenta) at 60 minutes (Fig. 2k). This effect is also supported by the TEM images taken after 60 minutes, which show a high contrast difference in the outer layer compared to the inner layer of the shell, which indicates that the inside shell of the peanut has become thinner with time (Fig. 2g). The TEM images at 240 minutes show that the nanorod coming out of the shell has no holes in its structure (Fig. 2h and i). This means that the core of the structure, *i.e.*, the nanorod remains intact during the dealloying process. This is attributed to the lower concentration of Ag atoms (∼4%) on the nanorod, which hinders the dealloying process (Table S1†). This concentration-dependent dealloying behavior of Ag atoms is due to the parting limit of Ag–Au alloy, which requires Ag to be more than 55 at% in the starting alloy.[57] Due to low fractions of silver, nanorods do not participate in the dealloying process. We note that the amount of Ag and Au in these structures were calculated from the ICP-OES measurement and differs from the actual ratio of Ag and Au in the growth medium. The difference in the deposited amounts of Ag during the growth of nanorod (∼4% Ag) and overgrowth of peanut (∼75% Ag) was controlled by varying the pH of the growth medium.[50] During the formation of nanorod and peanut, the pH of the solution was maintained at pH 4 and pH 8, respectively. At low pH, Ag acts as a capping agent by underpotential deposition while at high pH (pH > 6), Ag co-deposits along with Au on the NS.[50] Here, the precise ratio of Ag to Au was achieved by maintaining the pH of the growth solution.

We confirmed the same diffusion of Ag atoms through High Angle Angular Dark Field–Scanning Transmission Electron Microscopy (HAADF-STEM) imaging of the nanorod, peanut, and broken shell peanut. Fig. 3a shows the nanorod with mainly Au (green) and minute concentration of Ag (red), while the peanut structure in Fig. 3b shows a high concentration of both Au and Ag. The broken shell peanut structure shows a high concentration of Ag present only on the outer shell while Au was present both on the shell and the nanorod (Fig. 3c). For clarity, HAADF-STEM was also performed for the nanostructures where nanorod has come out of the shell. Here, it is clearly visible that Ag is present on the shell structure while Au is present on both the shell and the nanorod structure (Fig. 3d). This further confirms that even during overgrowth, the composition of the core remains unaltered.

The process of dealloying can be further controlled by tuning the concentration of hydrochloride acid. The rate of dealloying was found to be faster at a higher concentration of HCl (Fig. S5†). To understand the role of H^+ and Cl^- ions in this diffusion process, we kept the peanut nanostructure in the presence of 0.33 M NaCl, where no change was observed in the peanut structure (Fig. S6a†). The same reaction was then performed in the presence of HBr, where a similar dealloying effect was observed (Fig. S6b†). This indicates that H^+ ions are likely responsible for inducing the dealloying effect in the peanut structure. We note that bulk Au and Ag have reduction potential well above that of hydrogen ($Au^+/Au = 1.69$ V, $Ag^+/Ag = 0.8$ V, $H^+/H = 0$ V, and $Na^+/Na = -2.71$ V) in the electrochemical series.[58,59] Therefore, both bulk Au and Ag does not react with HCl. However, Au and Ag nanoparticles are known to react with HCl to produce $AuCl_4^-$ and AgCl, respectively.[58,59] The higher reactivity of Au and Ag nanoparticles is attributed to the large surface to volume ratio and a large number of unsaturated dangling Au and Ag atoms on their surfaces that reduce the actual potential. Furthermore, the presence of surfactant- and halogen-containing salts (*e.g.*, CTAB and CTAC) is known to reduce the potential of metal nanoparticles.[58,60] In the case of the Au–Ag alloy, both Au and Ag can react with HCl to give $AuCl_4^-$ and AgCl, respectively. Since Au^{3+}/Au has a higher reduction potential than that of Ag^+/Ag, $AuCl_4^-$ formed during dealloying can further oxidize Ag from the NS and itself get reduced to Au^0 and get deposited on the NS. Ultimately, in the Au–Ag alloy, only Ag is dealloyed from the NS. The formation of AgCl was confirmed by measuring the extinction spectrum of the supernatant solution after centrifuging the broken shell peanut structure (Fig. S7†).[61] The additional deposition observed around the nanostructure in the HAADF image in Fig. 3c shows the presence of Ag and not Au. The presence of

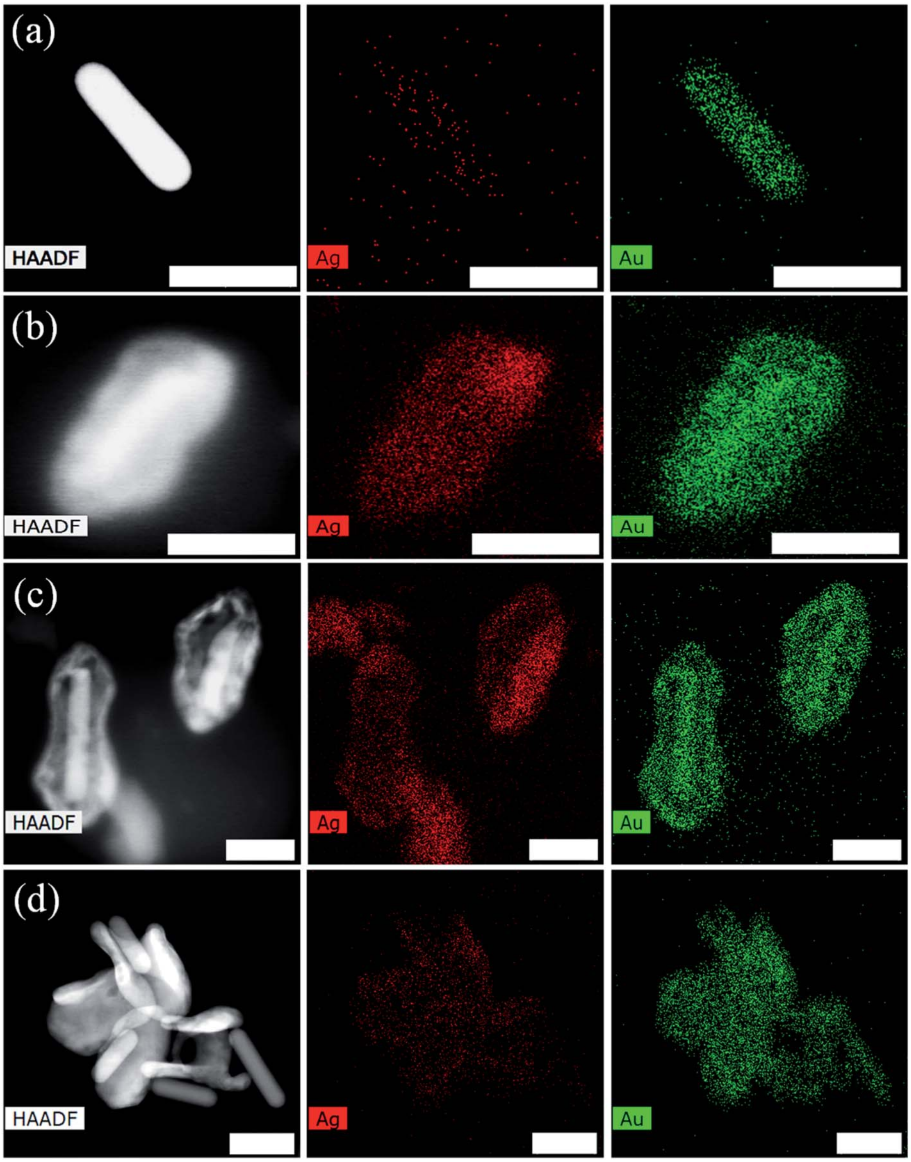

Fig. 3 High Angle Angular Dark Field (HAADF) image and their corresponding elemental mapping of Ag (red) and Au (green) on the nanorod (a), peanut (b), and broken shell peanut at 240 minutes (c) and (d). Scale bar is 40 nm.

only Ag may be attributed to AgCl, which is formed during the dealloying process. Note that Na^+ is not able to oxidize Ag to Ag^+ because the reduction potential of Ag^+/Ag in the NP is not low enough compared to the large negative reduction potential of Na^+/Na. Thus, the dealloying effect is only observed in the presence of H^+ and not with Na^+.

Now we will discuss the mechanism involved in the formation of the broken shell peanut structure. For simpler understanding, we have made three layers of atoms (refer to Scheme 2). The first two layers consist of both Au (yellowish-green) and Ag (magenta) atoms. These layers are formed during the formation of the peanut structure from the nanorod. The third layer of atoms consists of only Au atoms referring to the initial nanorod structure. At first, Ag ions diffuse out from the first layer. The Au atoms move and rearrange themselves to increase their coordination number on first layer by forming small islands (step 2). The hopping and rearrangement of Au atoms is indicated by the segregation of small holes (formed at 30 minutes, Fig. 2d) to one location, *i.e.*, near the tips of the peanut structure (Fig. 2f). The hopping and arrangement of Au atoms was also recently observed by the group of Chen using liquid-cell AC-STEM method.[55] The rearrangement of Au atoms also helps in the third step wherein Ag atoms from the second layer start diffusing out of these holes and voids, creating bigger voids in the internal structure. Then, no further diffusion takes place from the third layer due to the absence of Ag atoms (atomic percentage of Ag <4%) in the third layer. Ultimately, we are left with the outside shell of a peanut and a nanorod lying inside this shell.

Further, we probe the catalytic efficiency of the nanostructure in the reduction of 4-nitrophenol (4-NP) to 4-aminophenol (4-AP) in the presence of sodium borohydride. Metal

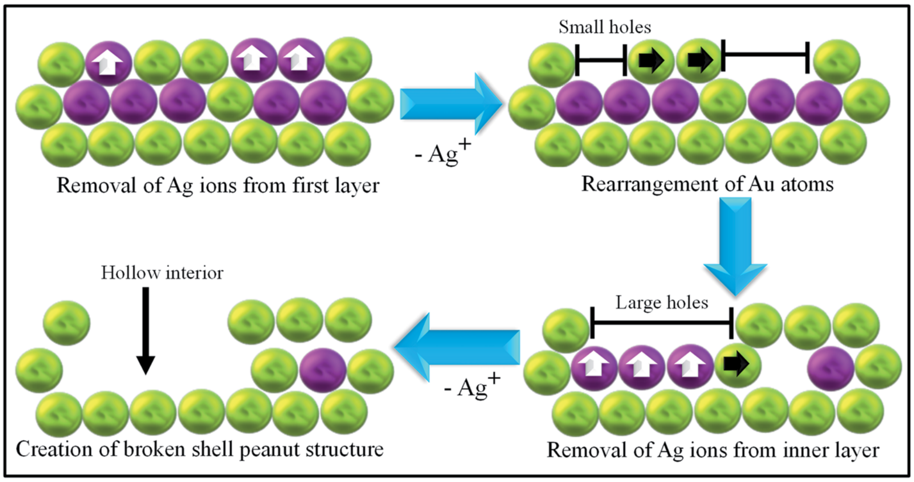

Scheme 2 Schematic depiction towards formation of broken shell peanut structure where golden yellow colour depicts Au and magenta depicts Ag atoms on the peanut structure.

NPs are known to catalyze this reaction by facilitating the electron transfer from BH_4^- to 4-NP.[62] The efficiency of the catalyst is determined by the rate of the reaction, where a higher rate would indicate a better catalyst. For this, we used five nanostructures, *i.e.*, nanorod (NR), peanut (BP 0), and broken shell peanut obtained at 30 minutes (BP 30, hole size 8 ± 4 nm), 60 minutes (BP 60, hole size 26 ± 7 nm), and 240 minutes (BP 240). To keep the concentration of different NS the same, the same amount of Au (calculated through ICP-OES) was added to the mixture of nitrophenol and sodium borohydride. It is important to note that throughout the transformation of the peanut to the broken shell peanut structure, the concentration of Au does not change. Hence, by keeping the same Au concentration, the same amount of nanostructure was added.

The reduction of 4-NP to 4-AP was studied *via* UV-Visible absorption spectroscopy (Fig. 4a and S8†), which showed a gradual decrease in the absorption peak at 400 nm as a function of the reaction time. This decrease in the 400 nm absorption peak as a function of time was monitored for the nanorod (NR), peanuts (BP 0), as well as the broken shell peanuts of different pore sizes (BP 30, BP 60, BP 240), and the results are given in Fig. 4b. It is quite evident that the decrease in the absorption peak intensity is faster for the broken shell peanuts than the pure peanuts and nanorod (BP 0 took 88 seconds (red), BP 30 took 48 seconds (magenta), BP 60 took 8 seconds (green), and BP 240 took 38 seconds (blue) to reduce the intensity at 400 nm to 0.1), making the broken shell peanuts better catalysts for this reaction.

To further understand the kinetics of the reaction, the reaction rate constants were measured for different nanostructures by taking I_0, *i.e.*, absorbance at 400 nm at time $T = 0$ minutes and I at various time intervals and plotting $\ln(I_0/I)$ *vs.* time (Fig. 4c). We find a linear relationship between $\ln(I_0/I)$ *vs.* time, suggesting pseudo-first-order reaction kinetics for all the nanostructures. This pseudo-first-order kinetics was also reported in the previous studies.[62] The rate constants were calculated from the slopes of the fitted lines (straight line) in Fig. 4c (0.00362 min^{-1} (NR), 0.0326 min^{-1} (BP 0), 0.05340 min^{-1} (BP 30), 0.0769 min^{-1} (BP 240), and 0.38812 min^{-1} (BP 60)). Fig. 4d shows the variation in the rate constant with different nanostructures. The calculated rate constants clearly showed that the broken shell peanuts (BP 60) have the highest catalytic activity with the rate constant 12 times higher than the pristine peanuts (BP 0) and 107 times more than the starting nanorods.

This observed difference in the catalytic activities among these nanostructures demonstrate the critical role of the hollow interior and the broken shell. The hollow interiors of the broken-shell peanuts contain a large number of uncoordinated atoms, which are known to provide better catalytic activities.[30] Increasing the number of uncoordinated atoms to achieve better catalytic activity was previously done by introducing structural anisotropy with corners and edges in the structure.[30,63] Furthermore, the holes and hollow interior also enhance the active surface area for catalysis. We also note that the selective removal of Ag atoms during the dealloying process may lead to a change in the co-ordination of the outer shell Au atoms, which may also enhance their catalytic activity.[64] It is interesting to note that BP 240 shows a decrease in the catalytic activity compared to BP 60. This reduced catalytic activity of BP 240 could be due to the collapse of the nanostructure, which ultimately reduces the resultant active catalytic surface area. We also note that the Ag concentration decreases from the peanuts to the broken shell peanuts in the order BP 0 > BP 30 > BP 60 > BP 240 (Fig. S4† with ICP-OES) and previous studies have indicated that both Au and Ag catalyze the conversions of 4-NP to 4-AP.[62] Thus, the decrease in the Ag concentrations will have a negative impact on the catalytic activities of broken shell peanuts, particularly for BP 240, which has the lowest silver concentration among the nanostructures studied herein. Here, the nanorod shows the least catalytic activity. This may be due to its smaller volume, less uncoordinated atoms, and low concentration of Ag compared to the anisotropic peanut and broken shell peanut structures. Thota *et al.* in their work found

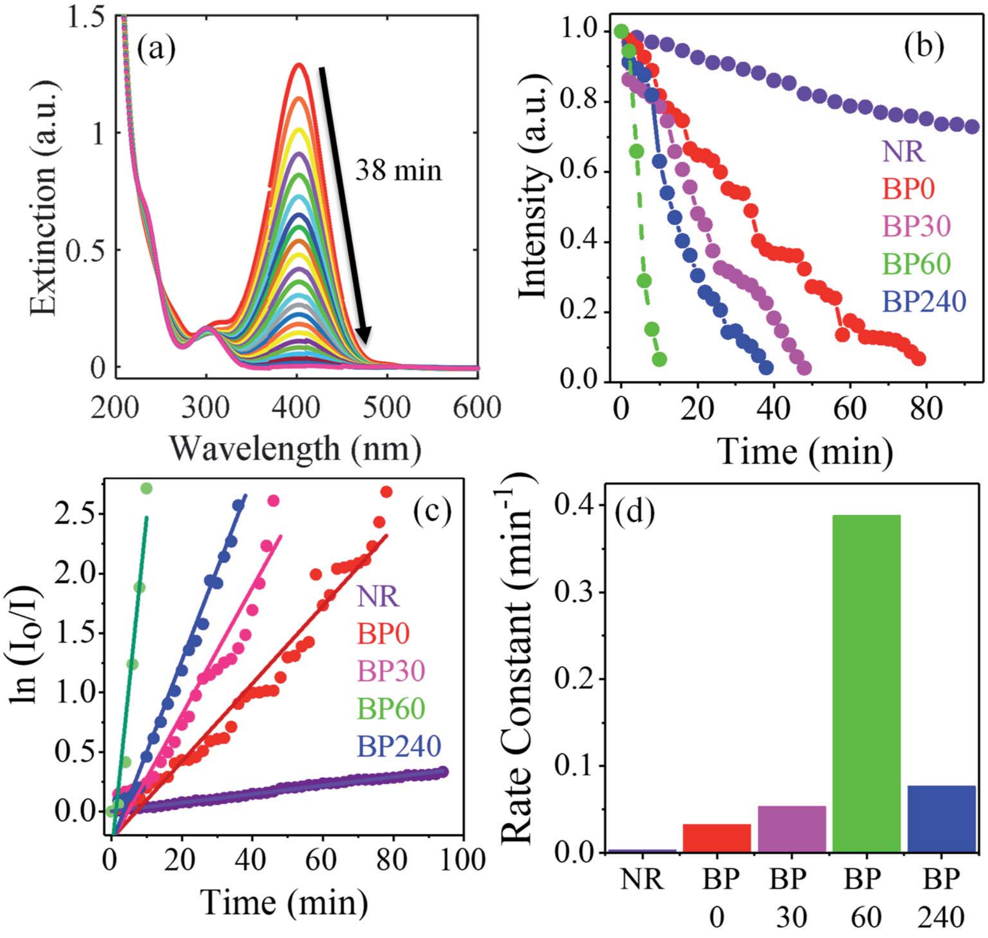

Fig. 4 (a) Time-dependent decrease in the intensity of the absorption peak at 400 nm monitored through UV-Visible absorption spectroscopy in the presence of BP 240. (b) The plot of change in the intensity of the absorption peak at 400 nm with time for different nanostructures. (c) Plot of $\ln(I_0/I)$ *vs.* time where linear dependence between $\ln(I_0/I)$ *vs.* time depicts pseudo first order reaction and the slope of the straight line determines the rate constant of the reaction. (d) Bar diagram showing the rate constant for different nanostructures: purple (nanorod, NR), red (peanut, BP 0), magenta (broken shell peanut 30 minutes, BP 30, pore size 8 ± 4 nm), green (broken shell peanut 60 minutes, BP 60, pore size 26 ± 7 nm), and blue (broken shell peanut 240 minutes, BP 240).

that rate constant for hollow nanorod ($k = 0.0257\ \text{s}^{-1}$) is 1.5 times higher than that of the solid nanorod ($k = 0.0169\ \text{s}^{-1}$).[12] Zeng *et al.* found nanocages ($k = 2.83\ \text{s}^{-1}$) to be 14 times better compared to the solid nanocubes ($0.20\ \text{s}^{-1}$).[27] In our case, the broken shell peanut (BP 60, $k = 0.38812\ \text{min}^{-1}$) shows 12 times more efficiency compared to the peanut ($k = 0.0326\ \text{min}^{-1}$) and 107 times than the nanorod ($k = 0.00362\ \text{min}^{-1}$) (Table S2†). Further, the catalysts were found to be stable even after the catalytic reaction with no changes in the geometry of the NPs (Fig. S9†).

5 Conclusion

In conclusion, we demonstrated the formation of a bimetallic core–shell AuAg@Au peanut structure and its transformation to the hollow core–shell broken shell peanut structure. This transformation happens in the presence of HCl, which is responsible for the formation of the broken shell peanut structure through the dealloying effect. Further, the hole size of the structure is controlled by the quenching of the reaction at different time intervals of 30 and 60 minutes and obtaining a hole size of 8 ± 4 nm and 26 ± 7 nm. These structures were utilized in the catalytic reduction of 4-nitrophenol to 4-aminophenol. The broken shell peanut with a hole size of 26 ± 7 nm was found to be twelve times more efficient than the peanut structure in the reduction of 4-NP to 4-AP.

Conflicts of interest

The authors declare no competing financial interest.

Acknowledgements

We acknowledge financial support from Science and Engineering research board, India (project: EMR/2015/0013), DST NanoMission, India (project: SR/NM/NS-65/2016), and a seed grant from IIT Gandhinagar. VT would like to acknowledge Diptiranjal Paital for his help with the schematics and Dr Kritika Khulbe for STEM analysis.

References

1 H. Chen, L. Shao, Q. Li and J. Wang, Gold Nanorods and Their Plasmonic Properties, *Chem. Soc. Rev.*, 2013, **42**(7), 2679–2724.

2 P. Zijlstra and M. Orrit, Single Metal Nanoparticles: Optical Detection, Spectroscopy and Applications, *Rep. Prog. Phys.*, 2011, **74**(10), 106401.

3 J. Olson, S. Dominguez-Medina, A. Hoggard, L.-Y. Wang, W.-S. Chang and S. Link, Optical Characterization of Single Plasmonic Nanoparticles, *Chem. Soc. Rev.*, 2015, **44**(1), 40–57.

4 M. Mandal, N. R. Jana, S. Kundu, S. K. Ghosh, M. Panigrahi and T. Pal, Synthesis of Aucore-Agshell Type Bimetallic Nanoparticles for Single Molecule Detection in Solution by SERS Method, *J. Nanopart. Res.*, 2004, **6**(1), 53–61.

5 P. Ghosh, A. Kar, S. Khandelwal, D. Vyas, A. Q. Mir, A. L. Chakraborty, R. S. Hegde, S. Sharma, A. Dutta and S. Khatua, Plasmonic CoO-Decorated Au Nanorods for Photoelectrocatalytic Water Oxidation, *ACS Appl. Nano Mater.*, 2019, **2**(9), 5795–5803.

6 P. Jena, M. Bhattacharya, G. Bhattacharjee, B. Satpati, P. Mukherjee, D. Senapati and R. Srinivasan, Bimetallic Gold-Silver Nanoparticles Mediate Bacterial Killing by Disrupting the Actin Cytoskeleton MreB, *Nanoscale*, 2020, **12**(6), 3731–3749.

7 A. S. K. Hashmi, Homogeneous Catalysis by Gold, *Gold Bull.*, 2004, **37**(1–2), 51–65.

8 M. Xiao, Z. Wang, M. Lyu, B. Luo, S. Wang, G. Liu, H. M. Cheng and L. Wang, Hollow Nanostructures for Photocatalysis: Advantages and Challenges, *Adv. Mater.*, 2018, **1801369**, 1–23.

9 A. S. K. Hashmi and M. Rudolph, Gold Catalysis in Total Synthesis, *Chem. Soc. Rev.*, 2008, **37**(9), 1766–1775.

10 R. Sardar, A. M. Funston, P. Mulvaney and R. W. Murray, Gold Nanoparticles: Past, Present, and Future, *Langmuir*, 2009, **25**(24), 13840–13851.

11 N. Dimitratos, J. A. Lopez-Sanchez and G. J. Hutchings, Selective Liquid Phase Oxidation with Supported Metal Nanoparticles, *Chem. Sci.*, 2012, **3**(1), 20–44.

12 S. Thota, S. Chen and J. Zhao, An Unconventional Mechanism of Hollow Nanorod Formation: Asymmetric Cu Diffusion in Au-Cu Alloy Nanorods during Galvanic Replacement Reaction, *Chem. Commun.*, 2016, **52**(32), 5593–5596.

13 A. Wittstock, J. Biener and M. Bäumer, Nanoporous Gold: A New Material for Catalytic and Sensor Applications, *Phys. Chem. Chem. Phys.*, 2010, **12**(40), 12919–12930.

14 X. Guo, W. Ye, H. Sun, Q. Zhang and J. Yang, A Dealloying Process of Core-Shell Au@AuAg Nanorods for Porous Nanorods with Enhanced Catalytic Activity, *Nanoscale*, 2013, **5**(24), 12582–12588.

15 Y. Choi, S. Hong, L. Liu, S. K. Kim and S. Park, Galvanically Replaced Hollow Au-Ag Nanospheres: Study of Their Surface Plasmon Resonance, *Langmuir*, 2012, **28**(16), 6670–6676.

16 R. Rajendra, P. Bhatia, A. Justin, S. Sharma and N. Ballav, Homogeneously-Alloyed Gold-Silver Nanoparticles as per Feeding Moles, *J. Phys. Chem. C*, 2015, **119**(10), 5604–5613.

17 Y. Park, C. Lee, S. Ryu and H. Song, *Ex Situ* and *in Situ* Surface Plasmon Monitoring of Temperature-Dependent Structural Evolution in Galvanic Replacement Reactions at a Single-Particle Level, *J. Phys. Chem. C*, 2015, **119**(34), 20125–20135.

18 S. W. Chee, S. F. Tan, Z. Baraissov, M. Bosman and U. Mirsaidov, Direct Observation of the Nanoscale Kirkendall Effect during Galvanic Replacement Reactions, *Nat. Commun.*, 2017, **8**(1), 1–8.

19 H. Jing and H. Wang, Structural Evolution of Ag-Pd Bimetallic Nanoparticles through Controlled Galvanic Replacement: Effects of Mild Reducing Agents, *Chem. Mater.*, 2015, **27**(6), 2172–2180.

20 N. Wiriyakun, K. Pankhlueab, S. Boonrungsiman and R. Laocharoensuk, Site-Selective Controlled Dealloying Process of Gold-Silver Nanowire Array: A Simple Approach towards Long-Term Stability and Sensitivity Improvement of SERS Substrate, *Sci. Rep.*, 2016, **6**(8), 1–11.

21 A. A. El Mel, R. Nakamura and C. Bittencourt, The Kirkendall Effect and Nanoscience: Hollow Nanospheres and Nanotubes, *Beilstein J. Nanotechnol.*, 2015, **6**(1), 1348–1361.

22 Y. Sun and Y. Xia, Alloying and Dealloying Processes Involved in the Preparation of Metal Nanoshells through a Galvanic Replacement Reaction, *Nano Lett.*, 2003, **3**(11), 1569–1572.

23 Y. Ridelman, G. Singh, R. Popovitz-Biro, S. G. Wolf, S. Das and R. Klajn, Metallic Nanobowls by Galvanic Replacement Reaction on Heterodimeric Nanoparticles, *Small*, 2012, **8**(5), 654–660.

24 X. Hong, D. Wang, S. Cai, H. Rong and Y. Li, Single-Crystalline Octahedral Au-Ag Nanoframes, *J. Am. Chem. Soc.*, 2012, **134**(44), 18165–18168.

25 A. K. Sasmal, J. Pal, R. Sahoo, P. Kartikeya, S. Dutta and T. Pal, Superb Dye Adsorption and Dye-Sensitized Change in Cu_2O-Ag Crystal Faces in the Dark, *J. Phys. Chem. C*, 2016, **120**(38), 21580–21588.

26 J. X. Wang, C. Ma, Y. Choi, D. Su, Y. Zhu, P. Liu, R. Si, M. B. Vukmirovic, Y. Zhang and R. R. Adzic, Kirkendall Effect and Lattice Contraction in Nanocatalysts: A New Strategy to Enhance Sustainable Activity, *J. Am. Chem. Soc.*, 2011, **133**(34), 13551–13557.

27 J. Zeng, Q. Zhang, J. Chen and Y. Xia, A Comparison Study of the Catalytic Properties of Au-Based Nanocages, Nanoboxes, and Nanoparticles, *Nano Lett.*, 2010, **10**(1), 30–35.

28 H. Wu, P. Wang, H. He and Y. Jin, Controlled Synthesis of Porous Ag/Au Bimetallic Hollow Nanoshells with Tunable Plasmonic and Catalytic Properties, *Nano Res.*, 2012, **5**(2), 135–144.

29 M. A. Mahmoud and M. A. El-Sayed, Time Dependence and Signs of the Shift of the Surface Plasmon Resonance Frequency in Nanocages Elucidate the Nanocatalysis Mechanism in Hollow Nanoparticles, *Nano Lett.*, 2011, **11**(3), 946–953.

30 C. W. Yen, M. A. Mahmoud and M. A. El-Sayed, Photocatalysis in Gold Nanocage Nanoreactors, *J. Phys. Chem. A*, 2009, **113**(16), 4340–4345.

31 A. Genç, J. Patarroyo, J. Sancho-Parramon, N. G. Bastús, V. Puntes and J. Arbiol, Hollow Metal Nanostructures for Enhanced Plasmonics: Synthesis, Local Plasmonic Properties and Applications, *Nanophotonics*, 2017, **6**(1), 193–213.

32 C. Zhu, D. Du, A. Eychmüller and Y. Lin, Engineering Ordered and Nonordered Porous Noble Metal Nanostructures: Synthesis, Assembly, and Their Applications in Electrochemistry, *Chem. Rev.*, 2015, **115**(16), 8896–8943.

33 S. W. Chee, Z. M. Wong, Z. Baraissov, S. F. Tan, T. L. Tan and U. Mirsaidov, Interface-Mediated Kirkendall Effect and Nanoscale Void Migration in Bimetallic Nanoparticles during Interdiffusion, *Nat. Commun.*, 2019, **10**(1), 1–8.

34 H. J. Fan, U. Gösele and M. Zacharias, Formation of Nanotubes and Hollow Nanoparticles Based on Kirkendall and Diffusion Processes: A Review, *Small*, 2007, **3**(10), 1660–1671.

35 X. Li, Q. Chen, I. McCue, J. Snyder, P. Crozier, J. Erlebacher and K. Sieradzki, Dealloying of Noble-Metal Alloy Nanoparticles, *Nano Lett.*, 2014, **14**(5), 2569–2577.

36 Z. Qi and J. Weissmüller, Hierarchical Nested-Network Nanostructure by Dealloying, *ACS Nano*, 2013, **7**(7), 5948–5954.

37 J. Feng and Y. Yin, Self-Templating Approaches to Hollow Nanostructures, *Adv. Mater.*, 2018, **1802349**, 1–14.

38 W. Wang, M. Dahl and Y. Yin, Hollow Nanocrystals through the Nanoscale Kirkendall Effect, *Chem. Mater.*, 2013, **25**(8), 1179–1189.

39 M. A. Mahmoud, D. O'Neil and M. A. El-Sayed, Hollow and Solid Metallic Nanoparticles in Sensing and in Nanocatalysis, *Chem. Mater.*, 2014, **26**(1), 44–58.

40 J. Liu, S. Z. Qiao, J. S. Chen, X. W. Lou, X. Xing and G. Q. Lu, Yolk/Shell Nanoparticles: New Platforms for Nanoreactors, Drug Delivery and Lithium-Ion Batteries, *Chem. Commun.*, 2011, **47**(47), 12578–12591.

41 D. Seo and H. Song, Asymmetric Hollow Nanorod Formation through a Partial Galvanic Replacement Reaction, *J. Am. Chem. Soc.*, 2009, **131**(51), 18210–18211.

42 E. C. Cho, P. H. C. Camargo and Y. Xia, Synthesis and Characterization of Noble-Metal Nanostructures Containing Gold Nanorods in the Center, *Adv. Mater.*, 2010, **22**(6), 744–748.

43 J. Huang, Y. Zhu, C. Liu, Y. Zhao, Z. Liu, M. N. Hedhili, A. Fratalocchi and Y. Han, Fabricating a Homogeneously Alloyed AuAg Shell on Au Nanorods to Achieve Strong, Stable, and Tunable Surface Plasmon Resonances, *Small*, 2015, **11**(39), 5214–5221.

44 X. Huang, I. H. El-Sayed, W. Qian and M. A. El-Sayed, Cancer Cell Imaging and Photothermal Therapy in the Near-Infrared Region by Using Gold Nanorods, *J. Am. Chem. Soc.*, 2006, **128**(6), 2115–2120.

45 B. N. Khlebtsov, V. A. Khanadeev, J. Ye and G. B. Sukhorukov, Overgrowth of Gold Nanorods by Using a Binary Surfactant Mixture, *Langmuir*, 2014, **30**(6), 1696–1703.

46 B. N. Khlebtsov, Z. Liu, J. Ye and N. G. Khlebtsov, Au@Ag Core/Shell Cuboids and Dumbbells: Optical Properties and SERS Response, *J. Quant. Spectrosc. Radiat. Transfer*, 2015, **167**, 64–75.

47 Q. Zhang, H. Jing, G. G. Li, Y. Lin, D. A. Blom and H. Wang, Intertwining Roles of Silver Ions, Surfactants, and Reducing Agents in Gold Nanorod Overgrowth: Pathway Switch between Silver Underpotential Deposition and Gold-Silver Codeposition, *Chem. Mater.*, 2016, **28**(8), 2728–2741.

48 Q. Zhang, Y. Zhou, E. Villarreal, Y. Lin, S. Zou and H. Wang, Faceted Gold Nanorods: Nanocuboids, Convex Nanocuboids, and Concave Nanocuboids, *Nano Lett.*, 2015, **15**(6), 4161–4169.

49 Y. F. Huang, Y. W. Lin and H. T. Chang, Growth of Various Au-Ag Nanocomposites from Gold Seeds in Amino Acid Solutions, *Nanotechnology*, 2006, **17**(19), 4885–4894.

50 V. Thambi, A. Kar, P. Ghosh, D. Paital, A. R. S. Gautam and S. Khatua, Synthesis of Complex Nanoparticle Geometries *via* PH-Controlled Overgrowth of Gold Nanorods, *ACS Omega*, 2019, **4**(9), 13733–13739.

51 W. Xie, L. Su, P. Donfack, A. Shen, X. Zhou, M. Sackmann, A. Materny and J. Hu, Synthesis of Gold Nanopeanuts by Citrate Reduction of Gold Chloride on Gold-Silver Core-Shell Nanoparticles, *Chem. Commun.*, 2009, **35**, 5263–5265.

52 X. Kou, S. Zhang, Z. Yang, C. K. Tsung, G. D. Stucky, L. Sun, J. Wang and C. Yan, Glutathione- and Cysteine-Induced Transverse Overgrowth on Gold Nanorods, *J. Am. Chem. Soc.*, 2007, **129**(20), 6402–6404.

53 J. Hee Song, F. Kim, D. Kim and P. Yang, Crystal Overgrowth on Gold Nanorods: Tuning the Shape, Facet, Aspect Ratio, and Composition of the Nanorods, *Chem.–Eur. J.*, 2005, **11**(3), 910–916.

54 J. Dey, B. Hazra and M. Chandra, Modulation of LSPR Spectra and Enhanced RI-Sensitivity through Symmetry Breaking in Hollow Gold Nanoprism, *J. Chem. Phys.*, 2019, **151**(11), 114706.

55 P. Liu, Q. Chen, Y. Ito, J. Han, S. Chu, X. Wang, K. M. Reddy, S. Song, A. Hirata and M. Chen, Dealloying Kinetics of AgAu Nanoparticles by *in situ* Liquid-Cell Scanning Transmission Electron Microscopy, *Nano Lett.*, 2020, **20**(3), 1944–1951.

56 R. Liquid, J. Erlebacher, M. J. Aziz, A. Karma and N. Dimitrov, *Nature Dealloying*, 2001, **410**(3), 5–8.

57 D. M. Artymowicz, J. Erlebacher and R. C. Newman, Relationship between the Parting Limit for De-Alloying and a Particular Geometric High-Density Site Percolation Threshold, *Philos. Mag.*, 2009, **89**(21), 1663–1693.

58 L. Li and Y. J. Zhu, High Chemical Reactivity of Silver Nanoparticles toward Hydrochloric Acid, *J. Colloid Interface Sci.*, 2006, **303**(2), 415–418.

59 H. Shi, H. Bi, B. Yao and L. Zhang, Dissolution of Au Nanoparticles in Hydrochloric Acid Solution as Studied by Optical Absorption, *Appl. Surf. Sci.*, 2000, **161**(1), 276–278.

60 Y. Xia, X. Xia and H. C. Peng, Shape-Controlled Synthesis of Colloidal Metal Nanocrystals: Thermodynamic *versus* Kinetic Products, *J. Am. Chem. Soc.*, 2015, **137**(25), 7947–7966.

61 Y. Rui, W. Zhao, D. Zhu, H. Wang, G. Song, M. T. Swihart, N. Wan, D. Gu, X. Tang, Y. Yang and T. Zhang, Understanding the Effects of NaCl, NaBr and Their

Mixtures on Silver Nanowire Nucleation and Growth in Terms of the Distribution of Electron Traps in Silver Halide Crystals, *Nanomaterials*, 2018, **8**(3), 1–15.

62 K. K. Haldar, S. Kundu and A. Patra, Core-Size-Dependent Catalytic Properties of Bimetallic Au/Ag Core-Shell Nanoparticles, *ACS Appl. Mater. Interfaces*, 2014, **6**(24), 21946–21953.

63 J. Park, T. Kwon, J. Kim, H. Jin, H. Y. Kim, B. Kim, S. H. Joo and K. Lee, Hollow Nanoparticles as Emerging Electrocatalysts for Renewable Energy Conversion Reactions, *Chem. Soc. Rev.*, 2018, **47**(22), 8173–8202.

64 S. Cao, F. F. Tao, Y. Tang, Y. Li and J. Yu, Size- and Shape-Dependent Catalytic Performances of Oxidation and Reduction Reactions on Nanocatalysts, *Chem. Soc. Rev.*, 2016, **45**(17), 4747–4765.